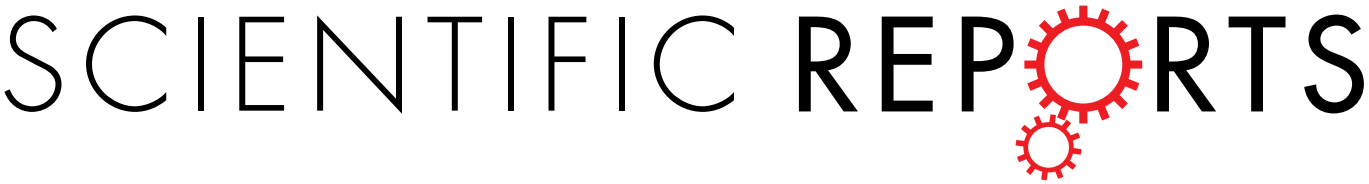

OPEN

New positive feedback mechanism between boundary layer meteorology and secondary aerosol formation during severe haze events

Received: 25 May 2017
Accepted: 3 April 2018
Published online: 17 April 2018

Quan Liu[1,2], Xingcan Jia[2], Jiannong Quan[2,3], Jiayun Li[4], Xia Li[1], Yongxue Wu[5], Dan Chen, Zifa Wang[6] & Yangang Liu[3]

Severe haze events during which particulate matter (PM) increases quickly from tens to hundreds of microgram per cubic meter in 1–2 days frequently occur in China. Although it has been known that PM is influenced by complex interplays among emissions, meteorology, and physical and chemical processes, specific mechanisms remain elusive. Here, a new positive feedback mechanism between planetary boundary layer (PBL), relative humidity (RH), and secondary PM (SPM) formation is proposed based on a comprehensive field experiment and model simulation. The decreased PBL associated with increased PM increases RH by weakening the vertical transport of water vapor; the increased RH in turn enhances the SPM formation through heterogeneous aqueous reactions, which further enhances PM, weakens solar radiation, and decreases PBL height. This positive feedback, together with the PM-Radiation-PBL feedback, constitutes a key mechanism that links PM, radiation, PBL properties (e.g. PBL height and RH), and SPM formation, This mechanism is self-amplifying, leading to faster PM production, accumulation, and more severe haze pollution.

China has been experiencing heavy air pollution in the past two decades, with frequent severe haze events[1,2]. During haze events, the mass concentration of fine particulate matter (smaller than 2.5 μm in aerodynamic diameter, $PM_{2.5}$) can reach as high as 600 $\mu g\,m^{-3}$[3–6]. Besides, the increase of $PM_{2.5}$ during haze events is steep, sometime by an order of magnitude in 1–2 days[3,7,8]. High emissions of atmospheric pollutants, including primary aerosols and their gas precursors, are thought as main causes of heavy air pollution in China[5,7,9]. Weakened atmospheric diffusion has also been considered to enhance the $PM_{2.5}$ accumulation because stable meteorological conditions favor the accumulation of primary and secondary pollutants[10]. Furthermore, the complex interplays among emissions, PBL meteorology, and atmospheric chemical processes make it more difficult to understand the formation of severe haze events[11–15]. A key player in the web of interplays is the PBL, which constitutes the lowest atmospheric layer. There is generally a barrier (very low turbulent mixing rate) at the top of the PBL to prevent particles being transported from the PBL to the free troposphere[16,17]. As a result, aerosol particles are mainly constrained in the PBL, and aerosol concentrations are anti-correlated with the PBL heights[11,17]. Furthermore, aerosol particles also influence the PBL stability[18–20] and PBL height[12,13] by decreasing the solar radiation reaching the Earth's surface[3,11,21] and turbulent mixing[14]. It has been recently found that aerosol particles can also affect the formation of secondary aerosols by changing photolysis rate and O_3 formation[22,23], and the involvement of heterogeneous aqueous reactions might make it more complex[24–28]. Despite these studies and some general

[1]Beijing Weather Modification Office, Beijing, China. [2]Institute of Urban Meteorology, Chinese Meteorological Administration, Beijing, China. [3]Brookhaven National Laboratory, Upton, NY, 11973, USA. [4]College of Atmospheric sciences, Lanzhou University, Lanzhou, China. [5]Beijing Meteorological Bureau, Beijing, China. [6]Institute of Atmospheric Physics, Chinese Academy of Sciences, Beijing, China. Quan Liu and Xingcan Jia contributed equally to this work. Correspondence and requests for materials should be addressed to J.Q. (email: jnquan@ium.cn) or Z.W. (email: zifawang@mail.iap.ac.cn) or Y.L. (email: lyg@bnl.gov)

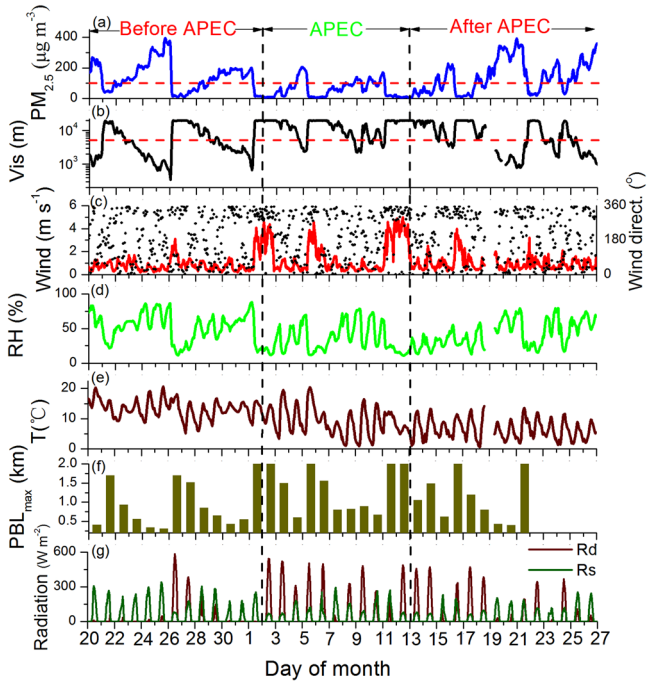

Figure 1. Temporal variations of $PM_{2.5}$ mass concentration (**a**), visibility (**b**), wind (**c**), relative humidity (RH) (**d**), temperature (**e**), daily maximum PBL height (PBL_{max}), averaged with data between 13:00–15:00 (**f**), and direct and scattered solar radiation (**g**). The temporal resolution of variables is 1 h, except for the PBL.

understanding, physical-chemical mechanisms underlying the complex interplays remained largely elusive in such heavily-polluted environments as those encountered in China.

During the 2014 Asia-Pacific Economic Cooperation (APEC) summit, a series of emission control measures[8,29] was implemented during 2–12 Nov. 2014 to ensure good air quality, providing a unique opportunity to understand the effect of emission reduction and the complex interplays between aerosols, meteorology (wind, radiation, PBL, and RH), and atmospheric chemical processes. We capitalized on this opportunity by organizing a comprehensive field campaign in the urban area of Beijing. A number of quantities, including atmospheric visibility, $PM_{2.5}$ mass concentration, chemical composition of non-refractory submicron particles (NR-PM_1), and PBL structure, were measured simultaneously, together with key meteorological variables (temperature, RH, pressure, wind, and solar radiation). This paper analyzes the data and presents the major findings from this campaign.

Results and Discussion

The comprehensive field campaign was conducted from 20 Oct. to 26 Nov. 2014 at the Baolian (BL) meteorological station, China Meteorological Administration (CMA) (39°56′N, 116°17′E). For comparative analysis, the period of 2–12 Nov., when the strict emission control was imposed, is chosen to represent the APEC period; whereas the periods before (20 Oct.–1 Nov.) and after (13–26 Nov.) the APEC are used to represent the non-APEC period. A total of 7 haze events (2 during the APEC and 5 during the non-APEC periods) occurred during the field campaign (haze events are defined as visibility being less than 5 km and RH less than 90%). Fig. 1 shows the temporal variations of the key variables during the whole field campaign. The $PM_{2.5}$ concentration (Fig. 1a) and visibility (Fig. 1b) exhibited a clear cycle of 4–7 days. Before each haze episode, strong northwest wind brought clear air to Beijing with abrupt decrease of aerosols and increase of visibility. After that, wind decreased and pollutants began to accumulate until the arrival of next clean northwest air at the end of the haze event (Fig. 1c). The peak $PM_{2.5}$ concentration reached 150–400 $\mu g\,m^{-3}$ (Fig. 1a) and visibility decreased to 1–3 km correspondingly (Fig. 1b). There were concurrent co-variations of other key variables during the haze events. For example, RH increased (Fig. 1d); the surface direct solar radiation (R_d) and total surface solar radiation decreased whereas the diffuse solar radiation (R_s) increased (Fig. 1g). The increased RH further decreased visibility by enhancing hygroscopic growth of aerosol particles[30,31].

High PM reduces PBL height. Aerosol particles modify radiative fluxes by scattering and absorption of solar radiation and, to a lesser extent, by absorption and emission of thermal infrared radiation[32]. Observations indicate that surface total solar radiation decreases from 243 $W\,m^{-2}$ to 149 $W\,m^{-2}$, with a decrease rate of 39%, when $PM_{2.5}$ increases from $<75\,\mu g\,cm^{-3}$ ($40\pm17\,\mu g\,cm^{-3}$) to $\geq75\,\mu g\,cm^{-3}$ ($187\pm81\,\mu g\,cm^{-3}$) (Fig. 2a), which is consistent with the calculated aerosol radiative forcing over North China Plain[13]. To see the radiative effect of aerosols on temperature profile, the sounding data are partitioned into two groups of high (HA) and low (LA) aerosols (Fig. 2b,c). The HA and LA groups represent the averages of all samples with the ground $PM_{2.5}$ $\geq75\,\mu g\,cm^{-3}$ and $PM_{2.5}$ $<75\,\mu g\,cm^{-3}$, respectively. A comparison of the temperature profiles reveals that low layer (<1 km) temperature decreased by 3.2 °C under HA while high layer (>1 km) temperature increased by 2.4 °C,

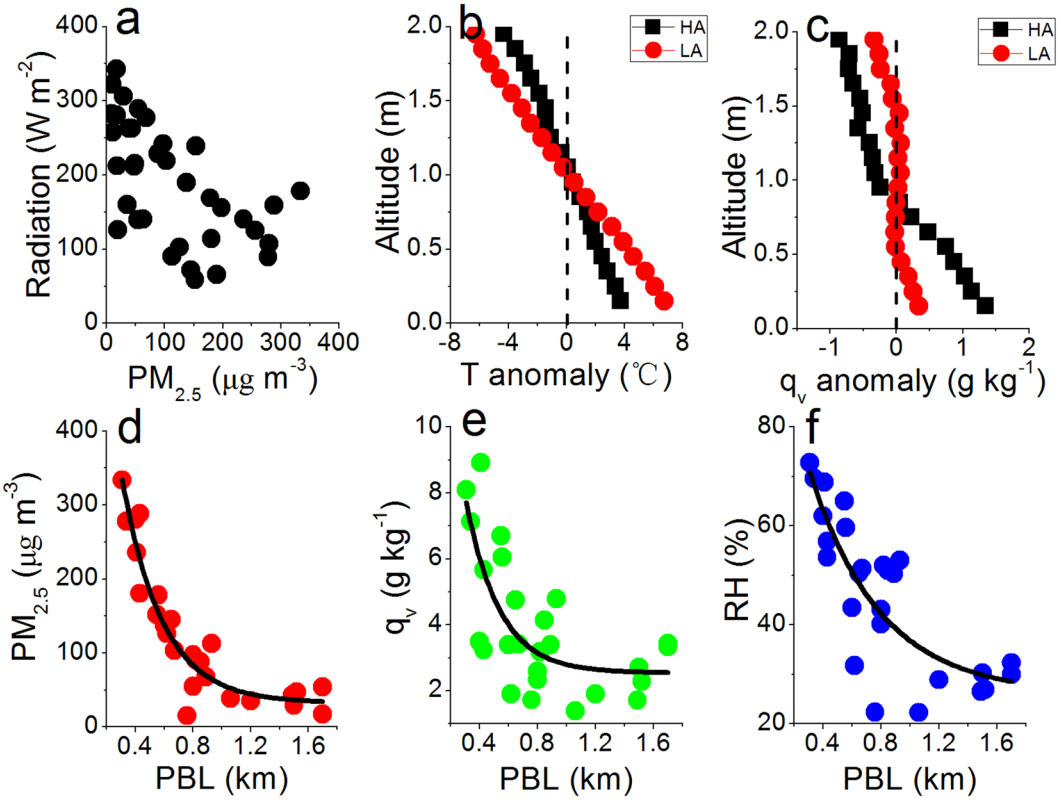

Figure 2. Relationships of radiation to $PM_{2.5}$ (**a**), profiles of temperature anomaly (**b**) and water vapor maxing ratio (q_v) anomaly (**c**) under high (HA, $PM_{2.5} \geq 75\,\mu g\,cm^{-3}$) and low aerosols (LA, $PM_{2.5} < 75\,\mu g\,cm^{-3}$), and relationships of $PM_{2.5}$ (**d**), q_v (**e**), RH (**f**) to PBL.

suggesting that atmosphere become more stable under high aerosols. A decreased downwelling direct solar radiation, together with stabilized atmosphere, could reduce turbulence kinetic energy[11,33] under high aerosols. The latter is the dominant factor that influences the development of the planetary boundary layer (PBL). As a result, the increased aerosols reduce PBL height. The daily maximum PBL height (PBL_{max}), averaged with data between 13:00–15:00, decreased from 1.3 to 0.6 km when ground $PM_{2.5}$ increased from $< 75\,\mu g\,cm^{-3}$ to $\geq 75\,\mu g\,cm^{-3}$.

Suppressed PBL enhances RH. There is generally a barrier (very low turbulent mixing rate) at the top of the PBL to prevent pollutants and water vapor being transported across from the PBL to the free troposphere[16,17]. As a result, aerosol particles, which origin mainly from ground emission, are mainly constrained in the PBL and aerosol concentration is anti-correlated with PBL height (Fig. 2d). Similar as aerosol particles, a large part of atmospheric water vapor inside PBL comes from surface evaporation[34] and anthropogenic emissions[35], especially under stable condition when haze event occurs. Hence, water vapor mixing ratio (q_v) is also anti-correlated with PBL height (Fig. 2e). To further verify this point, q_v profiles are analyzed (Fig. 2c). The vertical q_v gradient under high aerosols is much higher than under low aerosol, suggests that vertical transportation is suppressed and thus water vapor is accumulated in the lower layer (<1 km). The RH is closely related to water vapor; a high water vapor content corresponds to a high relative humidity under certain temperature. Therefore, the suppressed PBL caused by high aerosols increases RH inside PBL (Fig. 2f).

The $PM_{2.5}$ concentration, q_v, and RH increased with decreased PBL height, and their relationships appear non-linear. When PBL height was high, the change in $PM_{2.5}$, q_v and RH were weakly sensitive to PBL height. In contrast, when PBL height is low, the change in $PM_{2.5}$, q_v and RH were strongly sensitive to PBL height. The transition point corresponds to the PBL height of 0.8 km. For example, when PBL_{max} decreased from 1.6 km to 0.8 km, $PM_{2.5}$ increased from $38\,\mu g\,cm^{-3}$ to $75\,\mu g\,cm^{-3}$. The ratio of the changes between $PM_{2.5}$ and PBL height ($\Delta PM_{2.5}/\Delta PBL_{max}$) was -46 ($\mu g\,cm^{-3}\,km^{-1}$). In contrast, when PBL_{max} decreased from 0.8 km to 0.4 km, $PM_{2.5}$ increased from $75\,\mu g\,cm^{-3}$ to $250\,\mu g\,cm^{-3}$. The ratio of ($\Delta PM_{2.5}/\Delta PBL_{max}$) is -470 ($\mu g\,cm^{-3}\,km^{-1}$), which was about 10 times higher than the first value. The positive feedback of aerosol-PBL might act as a plausible explanation for above phenomenon. Based on the work of Petäjä[14], this feedback remains moderate at lower PM loadings, but becomes increasingly effective at higher PM loadings. High aerosols change the vertical temperature profile, cause the decay of turbulence and lowering of the PBL height. In turn, a direct consequence of the lowered PBL is increases in aerosols and water vapor since emissions were confined to a smaller volume. Therefore, in severe haze events with high aerosols, the positive feedback of aerosols-PBL further accelerates the accumulation of aerosol particles and water vapor inside PBL.

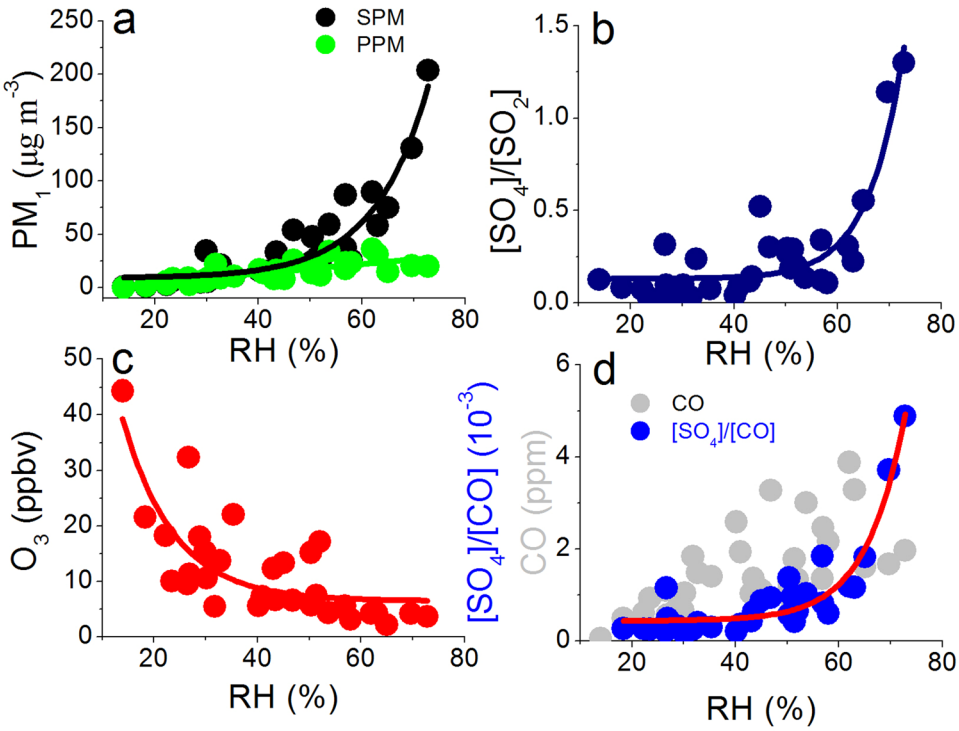

Figure 3. Relationships between RH and SPM and PPM (**a**), $[SO_4]/[SO_2]$ (**b**), O_3 (**c**), and $[SO_4]/[CO]$ and CO (**d**).

Enhanced RH accelerates SPM formation. Secondary particles, including sulfate (SO_4), nitrate (NO_3), ammonium (NH_4), and secondary organic aerosols (SOA) etc., contribute a large portion of $PM_{2.5}$ during severe haze events[3,6–8]. The conversion of gas precursors to particles is related to complex reaction mechanisms, including photochemistry reactions, heterogeneous aqueous reactions, and even cloud reactions[28]. For heterogeneous aqueous reactions, they are strongly related to RH. Under high RH, some aerosol particles likely experience hygroscopic growth, and their radii can be doubled, or approximate 8 times increase of particle volume[31], which provides an excellent substrate for heterogeneous aqueous reactions. To understand the contribution of heterogeneous aqueous reactions in haze events, relationships between RH and mass concentration of secondary PM (SPM), primary PM (PPM), and the sulfate production rate are analyzed (Fig. 3). The concentration ratios of sulfate to sulfur dioxide ($[SO_4]/[SO_2]$) is used as a proxy for the sulfate production rate[10,28]. The observations showed that the PPM concentration increased with RH in a moderate rate while the increase of SPM with RH is much more dramatic, especially when RH is higher than 60% (Fig. 3a), indicating accelerated SPM formation under high RH. For example, when RH increases from 50–60% to 60–70% the SPM concentration increases from 40 $\mu g\,m^{-3}$ to 88 $\mu g\,m^{-3}$, with an increase rate of 123%, about 4 factor of higher than the PPM increase (from 19 $\mu g\,m^{-3}$ to 26 $\mu g\,m^{-3}$, with an increase rate of 32%). The variation of sulfate production rate with RH further confirmed this result; The ratio ($[SO_4]/[SO_2]$) increases significantly when RH is higher than 60% (Fig. 3b), which is consistent with SPM variation. In contrast, the O_3 concentration is significantly reduced in this process, indicating a decrease of photochemistry capacity (Fig. 3c). The reduced photochemistry capacity and increased SPM production suggest the important contribution of heterogeneous aqueous reactions in secondary particles formation during severe haze events.

In addition to chemical processes, aerosol mass concentration is influenced simultaneously by meteorological processes. To estimate the relative contribution of chemical processes in the haze events, sulfate-CO ratio ($[SO_4]/[CO]$) is calculated. In this calculation, CO is selected as a inactive chemical tracer because of its long chemical lifetime. The chemical lifetime of CO is about a few months[36]. As a result, the variability of CO is mainly controlled by meteorological factors and sulfate-CO ratio can be estimated approximatively as the contribution of chemical processes[10]. As we can see from Fig. 3d that CO concentration increased with RH, suggests that they were affected simultaneously by the weakening atmospheric diffusion capacity in haze events. In addition, When RH was lower than 40%, $[SO_4]/[CO]$ kept nearly constant, but increased with further increasing RH especially when RH is higher than 60%, in consistence with the trend of sulfate production rate as a function of RH. Aerosol particles begin hygroscopic growth around 40% based on previous studies[37]. After that, the hygroscopic growth factor increased exponentially. The consistence of sulfate production rate to RH with aerosol hygroscopic growth further supports the role of heterogeneous aqueous reactions in SPM formation. Therefore, it is safe to conclude that heterogeneous aqueous reactions play dominant contribution in the formation of secondary particle formation during severe haze events; an increase of RH helps to accelerate the conversion of gas precursors to particles.

Feedback mechanism of PBL-RH-SPM. Based on above analysis, the low PBL height helps to enhance water vapor and hence RH inside PBL, which in turn enhances the conversion of gas precursors to particles

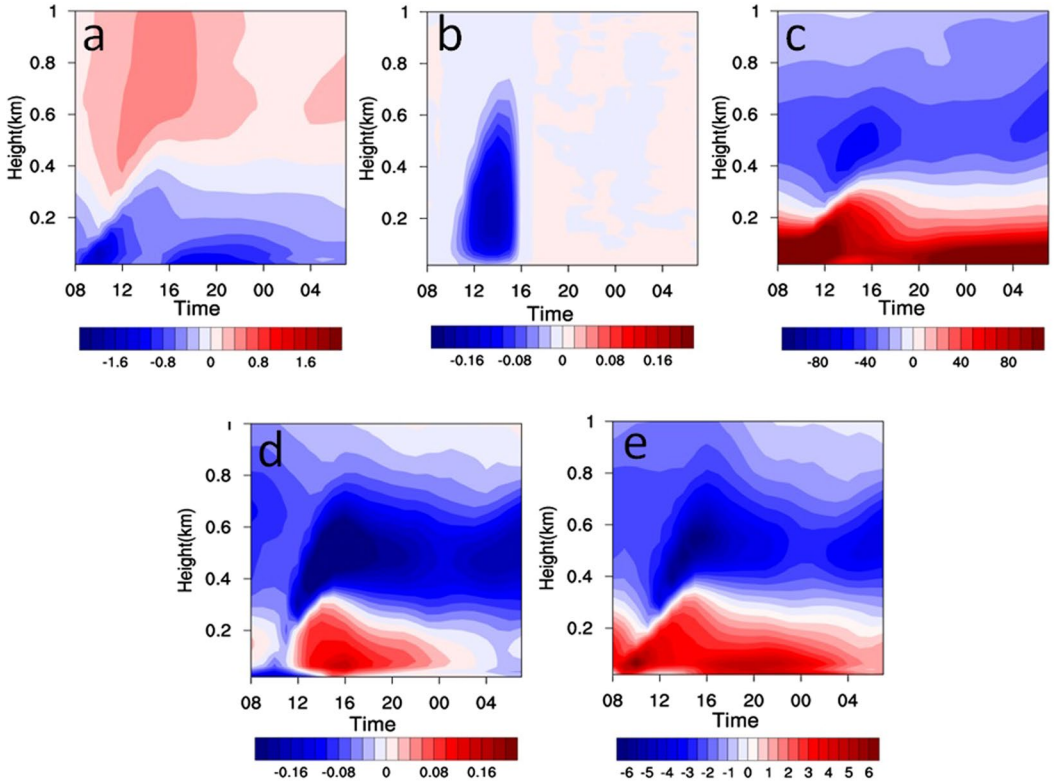

Figure 4. Vertical distribution of aerosol-radiation feedback induced diurnal difference (Scenario-4 - Scenario-3) in temperature (**a**, °C), TKE (**b**, J kg^{-1}), $PM_{2.5}$ concentration (**c**, μg m^{-3}), water vapor content (**d**, g kg^{-1}), and RH (**e**, %) for the study region during 18 to 21 December, 2016.

through heterogeneous aqueous reactions, further increasing PM concentration. The increased PM could further decrease PBL height due to the positive feedback of PM-radiation-PBL[11,12,14]. Furthermore, increased RH induces hygroscopic growth and an increase of aerosol particle size[30,31], which magnifies their effects on radiation and further decrease of PBL height. These results collectively suggest a plausible positive PBL-RH-SPM-PM feedback mechanism in haze events. This feedback mechanism, together with the positive feedback mechanism of PM-radiation-PBL[11,12,14], constitute a comprehensive positive loop of feedback mechanisms that links PM, radiation, PBL properties (e.g. PBL height and RH), and SPM formation, which could rapidly enhance PM in severe haze events.

According to this feedback loop, the formation of severe haze events can be summarized as follows: in the beginning of haze events, PM concentration and RH are low, and daytime PBL height is high. Weakened transport triggered by stagnant weather conditions leads to the PM accumulation. Increased PM suppresses the development of PBL by weakening solar radiation, leading to lower PBL height. Suppressed PBL helps to increase PM and RH, which induces hygroscopic growth of aerosol particles, further magnifies their effect on radiation and decrease of PBL height. Increased RH further enhances the formation of SPM through heterogeneous aqueous reactions.

The emission control during the APEC period provides a unique opportunity to evaluate the proposed feedback mechanisms. The mean APEC $PM_{2.5}$ concentration was 61 μg m^{-3}, decreased by 58% compared to that during the non-APEC period (144 μg m^{-3}, figure S1(a)). The decrease of $PM_{2.5}$ during the APEC period led to the corresponding increases of solar radiation (47%, figure S1(c)) and hence PBL_{max} height, which increased to 1.35 km during the APEC relative to 0.99 km in the non-APEC correspondingly (figure S1(d)). In the haze events, PBL_{max} decreased from 2.0 to 0.6–0.8 km during the APEC, as compared to 0.3–0.4 km during the non-APEC. The averaged RH decreased from 49% in the non-APEC to 37% in the APEC (figure S1(d)). The decrease in RH during the APEC slowed down the transfer of precursors to SPM. The fraction of SPM in $NR\text{-}PM_1$ decreased from 84% before the APEC to 62% in the APEC period (figure S2), indicating a slowdown of the chemical conversion of gaseous precursors to aerosols and helped to further decrease the $PM_{2.5}$ concentration in the APEC.

Model simulation. To further understand the feedback mechanisms and quantitatively estimate their contributions, model simulations are conducted with WRF-Chem[38]. The aerosol radiation effect, photochemistry, and heterogeneous reactions are considered, among other processes, in the simulations. Briefly, four simulations were conducted to investigate aerosols radiation (AR) effect and heterogeneous reactions. The analysis of the simulations shows that AR effect cools the lower PBL while warms the upper PBL (Fig. 4a), enhancing atmospheric stability. In this process, the turbulence kinetic energy (TKE) in the lower PBL also decreases (Fig. 4b). The combined thermodynamic and dynamic variations caused by AR effect suppress the PBL development and

its height decreases correspondingly (Fig. S3). The decreased PBL height (PBLH) weakens the vertical diffusion of aerosols, resulted in more aerosols in the lower atmosphere (Fig. 4c). Similar as aerosols, the decreased PBLH also alters the water vapor profile and more water vapor is accumulated in the lower atmosphere (Fig. 4d). The combined role of increased water vapor and decreased temperature result in higher RH in the lower atmosphere (Fig. 4e). The increased RH will promote the aerosol heterogeneous reactions and increase aerosol concentration correspondingly, which further enhances the aerosol radiation effect.

To quantitatively identify the contributions of AR effect and heterogeneous reactions, some key variables in the four simulations are compared, including shortwave radiation (SW), temperature, TKE, PBLH, RH, and $PM_{2.5}$ (Fig. S3). When AR effect is included (Scenario 2 - Scenario 1), the SW, temperature, TKE, and PBLH decrease by $69\,W\,m^{-2}$, 0.7 °C, $0.01\,J\,kg^{-1}$, and 147 m, respectively, while RH and $PM_{2.5}$ increased by 3% and $56\,\mu g\,m^{-3}$ respectively. When heterogeneous reactions are considered (Scenario 3 - Scenario 1), the $PM_{2.5}$ increases by $63\,\mu g\,m^{-3}$. When both AR effect and heterogeneous reactions are included simultaneously (Scenario 4 - Scenario 1), $PM_{2.5}$ increases by $179\,\mu g\,m^{-3}$. Several points are noteworthy from the simulations. First, the simulated $PM_{2.5}$ concentration is consistent with the observation when both AR effect and heterogeneous reactions are included, which are $275\,\mu g\,m^{-3}$ (observation) and $310\,\mu g\,m^{-3}$ (simulation) respectively, while $PM_{2.5}$ concentration is only $139\,\mu g\,m^{-3}$ when neither AR effect nor heterogeneous reactions is included (Scenario 1), much lower than the observation, indicating the important roles of AR effect and heterogeneous reactions on $PM_{2.5}$ in heavy air pollution events. Second, the $PM_{2.5}$ increase ($179\,\mu g\,m^{-3}$) when both AR effect and heterogeneous reactions are included (Scenario 4) is higher than the sum of $PM_{2.5}$ increase of individual AR effect ($56\,\mu g\,m^{-3}$) and heterogeneous reactions ($63\,\mu g\,m^{-3}$) are included, further supporting the significant role of the positive feedback mechanism proposed above.

Conclusion

A positive feedback mechanism between boundary layer meteorology and secondary particle formation is proposed based on the observational results. It is shown that in haze events the decreased PBL increases RH by weakening the diffusion of water vapor; the increased RH in turn enhances the SPM formation through heterogeneous aqueous reactions, which further increases PM. This feedback mechanism, together with the positive feedback mechanism of PM-radiation-PBL[11,12,14], constitutes a comprehensive positive loop of feedback mechanisms that links PM, radiation, PBL properties (e.g. PBL height and RH), and SPM formation, rapidly enhance PM in severe haze events: more PM leads to lower solar radiation, lower PBL height, higher RH, higher SPM formation, still higher PM and RH, and so on. For the same reason, reducing emissions will likely accelerate the decrease of the surface aerosol concentration. The new PBL-RH-SPM feedback mechanism, which has been largely ignored, should be used to improve air quality models, especially in heavy aerosol-polluted regions such as North China Plain.

Methods

Sampling and Observations. The comprehensive field campaign was conducted at the Baolian (BL) meteorological station, China Meteorological Administration (CMA) (39°56′N, 116°17′E). The measurements were taken from 20 Oct. to 26 Nov. 2014. The $PM_{2.5}$ mass concentration was measured with a R&P model 1400a Tapered Element Oscillating Microbalance (TEOM, Thermo Scientific Co., USA) instrument, with a 2.5 μm cyclone inlet and an inlet humidity control system. Atmospheric visibility was measured with a PWD20 (Vaisala Co., Finland), and meteorology variables were measured with WXT-510 (Vaisala Co., Finland). Solar radiations, including direct, scattered, and total radiation, were measured with TB-2-B series instruments (Huatron CO., China) that covers the wavelength of 0.3–3μm. A micro-pulse lidar (MPL-4B, Sigmaspace Co., USA) was employed to study the evolution of PBL. The PBL height is determined at the altitude where a sudden decrease in the scattering coefficient occurs[39–41]. A range of gaseous species including CO, O_3, NOx, and SO_2 were measured by TSI instruments (TSI Co., USA). The chemical composition of NR-PM_1 was measured with an Aerodyne compact Time-of-Flight Aerosol Mass Spectrometer (C-ToF-AMS).

AMS Data Analysis. The AMS data were analyzed for the mass concentrations and composition with the standard ToF-AMS data analysis software package (SQUIRREL version 1.52)[42,43]. A collection efficiency (CE) factor of 0.5 was introduced to account for the particle loss, mostly due to particle bounce at the vaporizer[44,45]. The values of relative ionization efficiency (RIE) used in this study were 1.2 for sulfate, 1.1 for nitrate, 1.3 for chloride and 1.4 for organics[45]. The RIE value of 4.0 was used for ammonium based on the analysis of pure NH_4NO_3 particles. The PMF (Positive Matrix Factorization) analysis[46] was performed on the organics mass spectra (m/z 12–300) following the procedures described in Ulbrich *et al.*[47]. In this study, organic aerosols were differentiated into four components by PMF analysis, including hydrocarbon-like (HOA), cooking-related (COA), coal combustion (CCOA) and oxygenated (OOA) organic aerosols. HOA, COA and CCOA are used to represent primary organic aerosols (POA), and OOA is used to represent secondary organic aerosols (SOA). In this work, Chl and POA are used to represent primary PM (PPM); SO_4, NO_3, NH_4, and SOA are used to represent secondary PM (SPM).

Model Configurations. The Weather Research and Forecasting (WRF) model coupled with online chemistry (WRF-Chem) is based upon the non-hydrostatic WRF community model (http://www.wrf-model.org/index.php). Details of the WRF-Chem model are described by Grell *et al.*[38]. We used version 3.6.1 in this study. The Morrison microphysical scheme[48] and the Grell–Devenyi ensemble cumulus parameterization[49] are used. The Noah parameterization is used to represent land surface processes and MYJ scheme to represent boundary layer turbulent mixing. The aerosol-radiation interaction is simulated with the Rapid Radiative Transfer Model (RRTMG)[50] for both SW and LW radiation as implemented by Zhao *et al.*[51]. The Carbon Bond Mechanism

version Z (CBMZ)[52] and Model for Simulating Aerosol Interactions and Chemistry (MOSAIC)[53] are used as the gas-phase and aerosol chemical mechanisms, respectively. MOSAIC uses a sectional approach to represent the aerosol size distribution with 4 and 8 size bins available in the public version of the code. In this study, we use 4 size bins with aerosols diameters ranging from 0.039–0.1, 0.1–1, 1–2.5, and 2.5–10 μm. The Fast-J photolysis scheme is used for photolytic rate calculations. New parameterizations of SO_2-to-H_2SO_4 and NO_2/NO_3-to-HNO_3 heterogeneous reaction rates that depend on relative humidity are applied[54]. The meteorological initial and boundary conditions are from the NCEP final analysis data (GFS). The lateral boundary conditions for chemistry and aerosol fields are based on the prescribed idealized profiles. The model domain, with 9 km horizontal grid spacing covers the North China Plain (223 × 202 grids), covers the urban clusters of northern and eastern China. There are 40 vertical layers from the surface to 50 hPa, with 10 layers below 500 m in order to simulate the haze event well. The simulation is from 15 Dec. to 21 Dec., 2016 and the first 3 days are treated as a spin-up period and are not used in analyses. Four scenarios of simulations are conducted to investigate the effects of aerosol radiation and heterogeneous reactions (see Table S1). In Scenario 1, no aerosol radiation and no heterogeneous reactions are included; In Scenario 2 aerosol radiation is included, together with the aerosol-radiation feedbacks. Scenario 3 only heterogeneous reactions; Scenario 4 considers both aerosol radiation and heterogeneous reactions. The emission inventory used in the four scenarios is the same. The differences between the four scenarios are used to isolate aerosols radiation effect and heterogeneous reactions effect.

References

1. Che, H., Zhang, X., Yang, L., Zhou, Z. & Qu, J. J. Horizontal visibility trends in China 1981–2005. *Geophys. Res. Lett.* **34**, 497–507 (2007).
2. Quan, J., Zhang, Q., He, H. & Liu, J. Analysis of the formation of fog and haze in North China Plain (NCP). *Atmos. Chem. Phys.* **11**, 11911–11937 (2011).
3. Quan, J. *et al*. Characteristics of heavy aerosol pollution during the 2012–2013 winter in Beijing, China. *Atmos. Environ.* **88**, 83–89 (2014).
4. Sun, Y. *et al*. Investigation of the sources and evolution processes of severe haze pollution in Beijing in January 2013. *J. Geophys. Res.* **119**, 2014JD021641 (2014).
5. Wang, Y. S. *et al*. Mechanism for the formation of the January 2013 heavy haze pollution episode over central and eastern China. *Sci. China Earth Sci.* **57**, 14–25 (2014).
6. Huang, R. J. *et al*. High secondary aerosol contribution to particulate pollution during haze events in China. *Nature* **514**, 218–222 (2014).
7. Guo, S. *et al*. Elucidating severe urban haze formation in China. *P. Natl. Acad. Sci. USA* **111**, 17373–17378 (2014).
8. Sun, Y. *et al*. "APEC Blue": Secondary Aerosol Reductions from Emission Controls in Beijing. *Sci. Rep.* **6**, 20668 (2016).
9. Chan, C. K. & Yao, X. Air pollution in megacities in China. *Atmos. Environ.* **42**, 1–42 (2008).
10. Zhang, Q. *et al*. Effects of meteorology and secondary particle formation on visibility during heavy haze events in Beijing, China. *Sci. Total Environ.* **502**, 578–584 (2015).
11. Quan, J. *et al*. Evolution of planetary boundary layer under different weather conditions, and its impact on aerosol concentrations. *Particuology* **11**, 34–40 (2013).
12. Wang, J. *et al*. Impact of aerosol–meteorology interactions on fine particle pollution during China's severe haze episode in January 2013. *Environ. Res. Lett.* **9**, 094002 (2014).
13. Gao, Y. *et al*. Modeling the feedback between aerosol and meteorological variables in the atmospheric boundary layer during a severe fog–haze event over the North China Plain. *Atmos. Chem. Phys.* **15**, 4279–4295 (2015).
14. Petäjä, T. *et al*. Enhanced air pollution via aerosolboundary layer feedback in China. *Sci. Rep.* **6**, 18998 (2016).
15. Zhang, L. *et al*. Sources and Processes Affecting Fine Particulate Matter Pollution over North China: An Adjoint Analysis of the Beijing APEC Period. *Environ. Sci. Technol.* **50**, 8731–8740 (2016).
16. Han, S. Q. *et al*. Impact measurements of nocturnal planetary boundary layer on urban air pollutants: from a 250-m tower over Tianjin, China. *J. Hazard. Mater.* **162**, 264–269 (2009).
17. Zhang, Q., Ma, X. C., Tie, X., Huang, M. & Zhao, C. Vertical distributions of aerosols under different weather conditions; analysis of *in-situ* aircraft measurements in Beijing, China. *Atmos. Environ.* **9**, 4621–4638 (2009).
18. Menon, S., Hansen, J., Nazarenko, L. & Luo, Y. Climate Effects of Black Carbon Aerosols in China and India. *Science* **297**, 2250–2253 (2002).
19. Zhao, C., Tie, X. & Lin, Y. A possible positive feedback of reduction of precipitation and increase in aerosols over eastern central China. *Geophys. Res. Lett.* **33**, L11814 (2006).
20. Bond, T. C. *et al*. Bounding the role of black carbon in the climate system: A scientific assessment. *J. Geophys. Res.* **118**, 5380–5552 (2013).
21. Yang, X., Zhao, C., Guo, J. & Wang, Y. Intensification of aerosol pollution associated with its feedback with surface solar radiation and winds in Beijing. *J. Geophys. Res.* **121**, 4093–4099 (2016).
22. Jacobson, M. Z. Studying the effects of aerosols on vertical photolysis rate coefficient and temperature profiles over an urban airshed. *J. Geophys. Res.* **103**, 10593–10604 (1998).
23. Li, G., Bei, N., Tie, X. & Molina, L. T. Aerosol effects on the photochemistry in Mexico City during MCMA-2006/MILAGRO campaign. *Atmos. Chem. Phys.* **11**, 5169–5182 (2011).
24. Zhang, Q. *et al*. Measured variability of SO_2 in an intensive fog event in the NCP region, China; evidence of high solubility of SO_2. *Particuology* **11**, 41–47 (2013).
25. Quan, J. *et al*. Effect of heterogeneous aqueous reactions on the secondary formation of inorganic aerosols during haze events. *Atmos. Environ.* **122**, 306–312 (2015).
26. Zheng, B. *et al*. Heterogeneous chemistry: a mechanism missing in current models to explain secondary inorganic aerosol formation during the January 2013 haze episode in North China. *Atmos. Chem. Phys.* **15**, 2031–2049 (2015).
27. Zheng, G. J. *et al*. Exploring the severe winter haze in Beijing: the impact of synoptic weather, regional transport and heterogeneous reactions. *Atmos. Chem. Phys.* **15**, 2969–2983 (2015).
28. Cheng, Y. *et al*. Reactive nitrogen chemistry in aerosol water as a source of sulfate during haze events in China. *Sci. Adv.* **2**, e1601530 (2016).
29. Tang, G. *et al*. Impact of emission controls on air quality in Beijing during APEC 2014: lidar ceilometer observations. *Atmos. Chem. Phys.* **15**, 12667–12680 (2015).
30. Cheng, Y. *et al*. Relative humidity dependence of aerosol optical properties and direct radiative forcing in the surface boundary layer at Xinken in Pearl River Delta of China: An observation based numerical study. *Atmos. Environ.* **42**, 6373–6397 (2008).
31. Liu, P. F. *et al*. Hygroscopic properties of aerosol particles at high relative humidity and their diurnal variations in the North China Plain. *Atmos. Chem. Phys.* **11**, 3479–3494 (2011).

32. Charlson, R. J. *et al*. Climate forcing by anthropogenic aerosols. *Science* **255**, 423–430 (1992).
33. Yu, H. B., Liu, S. C. & Dickinson, R. E. Radiative effects of aerosols on the evolution of the atmospheric boundary layer. *J. Geophys. Res.* **107**, 4142 (2002).
34. Arnfield, A. J. Two decades of urban climate research: a review of turbulence, exchanges of energy and water, and the urban heat island. *Int. J. Climatol.* **23**, 1–26 (2003).
35. Moriwaki, R., Kanda, M., Senoo, H., Hagishima, A. & Kinouchi, T. Anthropogenic water vapor emissions in Tokyo. *Water Resour. Res.* **44**, W11424 (2008).
36. Brasseur, G. P., Orlando, J. J. & Tyndall, G. S. Atmospheric chemistry and global change. New York: Oxford Univ. Press (1999).
37. Pan, X. L. *et al*. Observational study of influence of aerosol hygroscopic growth on scattering coefficient over rural area near Beijing mega-city. *Atmos. Chem. Phys.* **9**, 7519–7530 (2009).
38. Grell, G. A. *et al*. Fully coupled "online" chemistry within the WRF model. *Atmos. Environ.* **39**, 6957–6975 (2005).
39. Boers, R. & Eloranta, E. W. Lidar measurements of the atmospheric entrainment zone and potential temperature jump across the top of the mixed layer. *Bound.-Layer Meteor.* **34**, 357–375 (1986).
40. Brooks, I. M. Finding Boundary Layer Top: Application of a Wavelet Covariance Transform to Lidar Backscatter Profiles. *J. Atmos. Ocean. Technol.* **20**, 1092 (2003).
41. Cohn, S. A. & Angevine, W. M. Boundary Layer Height and Entrainment Zone Thickness Measured by Lidars and Wind-Profiling Radars. *J. Appl. Meteor.* **39**, 1233–1247 (2000).
42. Jimenez, J. L. *et al*. Ambient aerosol sampling using the Aerodyne Aerosol Mass Spectrometer. *J. Geophys. Res.* **108**, 8425 (2003).
43. DeCarlo, P. F. *et al*. Field-Deployable, High-Resolution, Time-of-Flight Aerosol Mass Spectrometer. *Anal. Chem.* **78**, 8281–8289 (2006).
44. Aiken, A. C. *et al*. Mexico City aerosol analysis during MILAGRO using high resolution aerosol mass spectrometry at the urban supersite (T0) – Part 1: Fine particle composition and organic source apportionment. *Atmos. Chem. Phys.* **9**, 6633–6653 (2009).
45. Canagaratna, M. R. *et al*. Chemical and microphysical characterization of ambient aerosols with the aerodyne aerosol mass spectrometer. *Mass Spectrom. Rev.* **26**, 185–222 (2007).
46. Paatero, P. & Tapper, U. Positive matrix factorization: A non-negative factor model with optimal utilization of error estimates of data values. *Environmetrics* **5**, 111–126 (1994).
47. Ulbrich, I. M., Canagaratna, M. R., Zhang, Q., Worsnop, D. R. & Jimenez, J. L. Interpretation of organic components from Positive Matrix Factorization of aerosol mass spectrometric data. *Atmos. Chem. Phys.* **9**, 2891–2918 (2009).
48. Morrison, H., Curry, J. A. & Khvorostyanov, V. I. A new double moment microphysics parameterization for application in cloud andclimate models. *Part I: Description. J. Atmos. Sci.* **62**, 1665–1677 (2005).
49. Grell, G. A. & Devenyi, D. A generalized approach to parameterizing convection combining ensemble and data assimilation techniques. *Geophys. Res. Lett.* **29**, 1693 (2002).
50. Iacono, M. J., Mlawer, E. J., Clough, S. A. & Morcrette, J. J. Impact of an improved longwave radiation model, RRTM, on the energy budget and thermodynamic properties of the NCAR community climate model, CCM3. *J. Geophys. Res.* **105**, 14873–14890 (2000).
51. Zhao, C., Leung, L. R., Easter, R., Hand, J. & Avise, J. Characterization of speciated aerosol direct radiative forcing over California. *J. Geophys. Res.* **118**, 2372–2388 (2013).
52. Zaveri, R. A. & Peters, L. K. A new lumped structure photochemical mechanism for large-scale applications. *J. Geophys. Res.* **104**, 30387–30415 (1999).
53. Zaveri, R. A., Easter, R. C., Fast, J. D. & Peters, L. K. Model for simulating aerosol interactions and chemistry (MOSAIC). *J. Geophys. Res.* **113**, D13204 (2008).
54. Chen, D., Liu, Z., Fast, J. & Ban, J. Simulations of sulfate–nitrate–ammonium (SNA) aerosols during the extreme haze events over northern China in October 2014. *Atmos. Chem. Phys.* **16**, 10707–10724 (2016).

Acknowledgements

This research is supported by National Key R&D Program of China (2017YFC0209604), National Natural Science Foundation of China (NSFC) (41505119), Basic R&D special fund for central level, scientific research institutes (IUMKY201709). Y.L. is supported by the US Department Energy's Atmospheric System Research (ASR) Program.

Author Contributions

J.Q. and Y.L. had the original idea. J.Q., Q.L., J.L., and X.J. conducted the observations of this campaign. X.J., D.C., and Z.W. performed the numerical simulation. Q.L., J.L., and X.J. analyzed pollutants data. X.L. analyzed boundary layer height. Y.W. analyzed radiation. J.Q. and Y.L. wrote the manuscript. All authors discussed the results and commented on the paper.

Additional Information

Supplementary information accompanies this paper at https://doi.org/10.1038/s41598-018-24366-3.

Competing Interests: The authors declare no competing interests.

Publisher's note: Springer Nature remains neutral with regard to jurisdictional claims in published maps and institutional affiliations.